Inorganic Chemistry

Article

pubs.acs.org/IC

Highly Distorted Uranyl Ion Coordination and One/Two-Dimensional Structural Relationship in the $Ba_2[UO_2(TO_4)_2]$ (T = P, As) System: An Experimental and Computational Study

Shijun Wu,[†,‡,§] Piotr M. Kowalski,[§,∥] Na Yu,[§] Thomas Malcherek,[⊥] Wulf Depmeier,[‡] Dirk Bosbach,[§] Shuao Wang,[#] Evgeny V. Suleimanov,[▽] Thomas E. Albrecht-Schmitt,*[,▲] and Evgeny V. Alekseev*[,§,■]

[†]Guangzhou Institute of Geochemistry, Chinese Academy of Sciences, 510640 Guangzhou, China

[‡]Institut für Geowissenschaften, Universität zu Kiel, 24118 Kiel, Germany

[§]Institute for Energy and Climate Research, Forschungszentrum Jülich GmbH, 52428 Jülich, Germany

[∥]JARA High-Performance Computing, Schinkelstraße 2, 52062 Aachen, Germany

[⊥]Mineralogisch-Petrographisches Institut, Universität Hamburg, 20146 Hamburg, Germany

[#]School of Radiological & Interdisciplinary Sciences, Soochow University, Suzhou 215123, China

[▽]Department of Chemistry, Lobachevsky State University of Nizhny Novgorod, 603950 Nizhny Novgorod, Russia

[▲]Department of Chemistry and Biochemistry, Florida State University, Tallahassee, Florida 32306, United States

[■]Institut für Kristallographie, RWTH Aachen University, 52056 Aachen, Germany

Supporting Information

ABSTRACT: Uranium compounds α-$Ba_2[UO_2(PO_4)_2]$ (**1**), β-$Ba_2[UO_2(PO_4)_2]$ (**2**), and $Ba_2[UO_2(AsO_4)_2]$ (**3**) were synthesized by H_3BO_3/B_2O_3 flux reactions, though boron is not incorporated into the structures. Phases **1** and **2** are topologically identical, but **1** is heavily distorted with respect to **2**. An unusual UO_7 pentagonal bipyramid occurs in **1**, exhibiting a highly distorted equatorial configuration and significant bending of the uranyl group, due to edge-sharing with one neighboring PO_4^{3-} tetrahedron. Compound **2** contains more normal square bipyramids that share corners with four neighboring PO_4^{3-} tetrahedra, but the uranyl cation UO_2^{2+} is tilted relative to the equatorial plane. Experimental evidence as well as density functional theory (DFT) calculations suggest that **1** is more stable than **2**. In theory, **1** and **2** can interconvert by forming/releasing the shared edge between the uranyl polyhedron and the phosphate tetrahedron. Similar fundamental building blocks in β-$Ba_2[UO_2(PO_4)_2]$ and $Ba_2[UO_2(AsO_4)_2]$ indicate a possible evolution of uranyl-based structures from chain to layer type and formation of an accretional series.

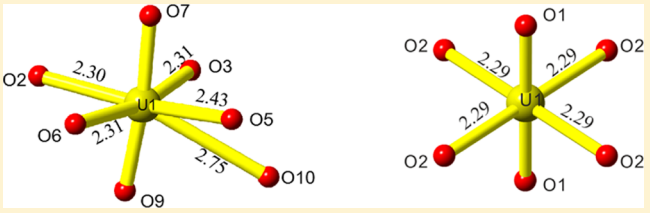

1. INTRODUCTION

The development of uranium solid-state chemistry enhances our understanding of mineralogical, geological, environmental, and technological issues of nuclear legacy.[1,2] In 2005, Burns[1] pointed out that at least 368 structures of inorganic uranyl compounds (including 89 minerals) were known. Since then, more than 250 additional inorganic uranyl compounds and minerals have been reported. Of all these structures, less than 20% contain chains of polyhedra, but more than 50% are layered structures. Although a novel approach for describing and classifying uranyl phases has been developed,[1,3] the relationship between uranyl chain structures and layered structures has not been fully realized.

Uranium(VI) is the most frequent valence state of uranium, in both natural uranyl minerals and synthetic compounds.[1,4] It is most commonly found to have short distances from two oxygen atoms to form an approximately linear uranyl ion (UO_2^{2+}) with an O═U═O angle close to 180°. The uranyl ion is typically coordinated by 4, 5, or 6 additional atoms (mostly O, but also C, N, etc.) in the equatorial plane to form a uranyl square, pentagonal, or hexagonal bipyramid, respectively. If appropriate, uranyl and equatorial oxygen atoms will be denoted O_{Ur} and O_{eq}, henceforth. Normally, the O_{eq} atoms within a given bipyramid form a flat plane with similar U—L (L = O, C, N, etc.) bond distances, which are usually longer than the U═O_{Ur} bonds in UO_2^{2+}. There are also some exceptions with unusual uranium coordination such as the uranium(VI) tetraoxido core, UO_4^{2-}, which is, however, more common for An^{VII} (An = Np, Pu).[5] In a uranium(VI) tetraoxido core square bipyramid, the equatorial bonds are shorter than the bonds within the UO_2^{2+} group.[1,3]

Uranyl phosphates and arsenates form two important groups in the family of uranyl minerals and mineral-like compounds. Because of the close relationship between the crystal chemistry of P(V) and As(V), their corresponding compounds often show

Received: April 25, 2014
Published: July 3, 2014

   dx.doi.org/10.1021/ic500965v | Inorg. Chem. 2014, 53, 7650−7660

Table 1. Crystallographic Data for 1, 2, and 3

	α-$Ba_2[UO_2(PO_4)_2]$ (**1**)	β-$Ba_2[UO_2(PO_4)_2]$ (**2**)	$Ba_2[UO_2(AsO_4)_2]$ (**3**)
molecular weight	734.63	734.63	822.53
color, shape	green, prism	yellow, prism	green, tablet
crystal system	triclinic	monoclinic	monoclinic
space group	$P\bar{1}$	$C2/m$	$P2_1/n$
a (Å)	6.774(2)	12.6020(9)	11.1033(5)
b (Å)	8.634(3)	5.3875(4)	8.7704(3)
c (Å)	9.030(4)	6.9527(3)	21.3572(8)
α (deg)	104.55(3)		
β (deg)	93.87(2)	102.621(4)	104.686(3)
γ (deg)	112.13(3)		
V (Å^3)	465.7(3)	460.64(5)	2011.83(14)
Z	2	2	4
T (K)	293	293	293
λ (Å)	0.710 73	0.710 73	0.710 73
max 2θ (deg)	56.56	56.56	57.56
ρ_{calcd} (g·cm^{-3})	5.239	5.297	5.431
μ(Mo Kα) (cm^{-1})	260.86	263.74	303.66
$R(F)$ for $F_o^2 > 2\sigma(F_o^2)^a$	0.0398	0.0315	0.0293
$R_w(F_o^2)^b$	0.1442	0.0716	0.0626

$^aR(F) = \sum||F_o| - |F_c||/\sum|F_o|$. $^bR(F_o^2) = [w(F_o^2 - F_c^2)^2/\sum w(F_o^4)]^{1/2}$.

similar crystal structures. A common topology is that of autunite/metautenite, where each uranyl square bipyramid is connected to four tetrahedra, and vice versa.[1] These phases are typically synthesized under hydrothermal conditions. Recently, Alekseev et al.[6a−f] and Renard et al.[6g] significantly extended the range of the uranyl phosphate/arsenate family by employing high-temperature solid-state reactions. Notably, all the phases were obtained by direct reactions of uranium oxide/nitrate, phosphorus/arsenic oxide, and $A^{1+,2+}$ (where A is, for example, alkali or alkaline earth elements) nitrates/carbonates without the use of fluxes.

Herein, we report on our study of a new U(VI)-based system with composition $Ba_2[UO_2(TO_4)_2]$ (T = P, As) synthesized from borate fluxes. The members of this system exhibit an unusual coordination environment of uranium(VI) in α-$Ba_2[UO_2(PO_4)_2]$ and an interesting 1D/2D structural relationship between β-$Ba_2[UO_2(PO_4)_2]$ and $Ba_2[UO_2(AsO_4)_2]$.

2. EXPERIMENTAL SECTION

2.1. Syntheses. $UO_2(NO_3)_2·6H_2O$ (Merck), $Ba(NO_3)_2$ (Alfa Aesar), $BaCO_3$ (Alfa Aesar), H_3BO_3 (Alfa Aesar), BPO_4 (Alfa Aesar), B_2O_3 (Alfa Aesar), and $NH_4H_2AsO_4$ (Alfa Aesar) were used as received. All syntheses used high-temperature fluxes and were performed in platinum crucibles. After the reactions were cooled to room temperature, singe crystals were harvested mechanically with a small knife and picked up with a stainless steel needle previous to crystallographic study. ***Caution!*** *Uranium is a radioactive element, and all operations have to be performed in the frame of radiation safety instructions.*

*2.1.3. Synthesis of α-$Ba_2[UO_2(PO_4)_2]$ (**1**).* $BaCO_3$ (197.34 mg, 1 mmol), B_2O_3 (34.81 mg, 0.5 mmol), BPO_4 (105.78 mg, 1 mmol), and $UO_2(NO_3)_2·6H_2O$ (125.5 mg, 0.25 mmol) (molar ratio Ba:B:P:U = 4:8:4:1) were ground in an agate mortar and placed into a platinum crucible. The mixture was heated to 1000 °C at a rate of 200 °C/h, kept at this temperature for 120 min, slowly cooled down (7 °C/h) to 300 °C, and finally quenched to room temperature. The product contained green prismatic crystals of **1** in a glassy mass.

*2.1.2. Synthesis of β-$Ba_2[UO_2(PO_4)_2]$ (**2**).* $BaCO_3$ (789.36 mg, 4 mmol), H_3BO_3 (245.52 mg, 4 mmol), BPO_4 (211.56 mg, 2 mmol), and $UO_2(NO_3)_2·6H_2O$ (1004.2 mg, 2 mmol) (molar ratio Ba:B:P:U = 2:3:1:1) were ground in an agate mortar and placed into a platinum crucible. The mixture was heated to 1300 °C at a rate of 180 °C/h, kept at this temperature for 2 h, slowly cooled down (7 °C/h) to 300 °C, and quenched. The product contained yellow prismatic crystals of **2** in a glassy mass.

*2.1.3. Synthesis of $Ba_2[UO_2(AsO_4)_2]$ (**3**).* $Ba(NO_3)_2$ (261.37 mg, 1 mmol), B_2O_3 (69.62 mg, 1 mmol), $NH_4H_2AsO_4$ (317.96 mg, 2 mmol), and $UO_2(NO_3)_2·6H_2O$ (125.5 mg, 0.25 mmol) (molar ratio Ba:B:As:U = 4:8:8:1) were ground in an agate mortar and placed into a platinum crucible. The mixture was heated to 1000 °C at a rate of 200 °C/h, kept at this temperature for 5 h, slowly cooled (5 °C/h) to 300 °C, and quenched. The resulting mixture contained green tablet crystals of **3** in a glassy mass.

2.2. Pure Phase Preparation of α-$Ba_2[UO_2(PO_4)_2]$. The only phase we were able to prepare in pure form was α-$Ba_2[UO_2(PO_4)_2]$. $Ba(NO_3)_2$, $UO_2(NO_3)_2·6H_2O$, and $NH_4H_2PO_4$ were taken in molar ratio equivalent to 2:1:2, ground, placed in a Pt crucible, and heated up to 850 °C for 12 h. This resulted in a yellowish powder of pure α-$Ba_2[UO_2(PO_4)_2]$. The other components, including nitrate, ammonium, and water, were volatilized during the heating. Several attempts to prepare the second polymorph, β-$Ba_2[UO_2(PO_4)_2]$, by use of lower or higher temperatures or B_2O_3 as a flux remained unsuccessful.

2.3. Powder X-ray Diffraction. We used standard room-temperature X-ray powder diffraction to test the purity of the obtained α-$Ba_2[UO_2(PO_4)_2]$. A Bruker D4 Endeavor diffractometer, 40 kV/40 mA, Cu Kα radiation (λ = 1.541 87 Å), equipped with a linear silicon strip LynxEye detector (Bruker) was used. Data were recorded in the range 2θ = 10−80° with 10 s/step and a step width of 0.02°. The aperture of the fixed divergence slit was set to 0.2 mm and the aperture of the receiving slit to 8.0 mm. In order to reduce possible fluorescence effects, the discriminator of the detector was set to an interval 0.16−0.25 V. The experimental and calculated powder patterns are provided in the Supporting Information (Figure S1). No phase other than **1** could be observed.

2.4. Crystallographic Studies. Crystals selected for data collection were mounted on a Nonius charge-coupled device (CCD) four-circle diffractometer. All data were collected by use of monochromatic Mo Kα radiation (λ = 0.710 73 Å). The unit-cell dimensions for all compounds (Table 1) were refined by least-squares techniques against the positions of all measured reflections. More than one hemisphere of data was collected for each crystal, and the three-dimensional (3D) data were integrated and corrected for Lorentz, polarization, and background effects by use of Eval14 procedures,[7] as implemented in the supporting programs for the diffractometer. Data were scaled and corrected for absorption effects by use of SADABS.[8] Additional information pertinent

dx.doi.org/10.1021/ic500965v | Inorg. Chem. 2014, 53, 7650−7660

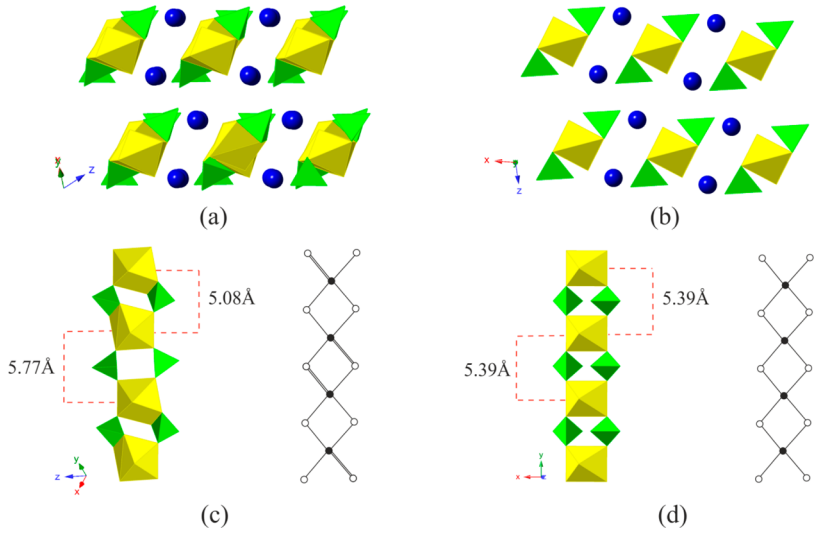

Figure 1. Polyhedral view of crystal structures of (a) **1** and (b) **2**, and (c, d) their infinite chain structures with topological representation. Uranium and phosphorus polyhedra are shown in yellow and green, respectively, while blue spheres represent Ba atoms.

to data collection is given in Table 1. The SHELXL-97 program was used for the determination and refinement of the structures.[9] The structures were solved by direct methods and refined to $R_1 = 0.0398$ for **1**, 0.0315 for **2**, and 0.0293 for **3**.

2.5. Computational Method. In order to supplement and better understand the experimentally obtained data we performed an ab initio investigation of the polymorphic structures of **1** and **2**. Calculations were performed by density functional theory (DFT), which is nowadays a widely used method for the computation of extended, many-particle systems such as the ones investigated here. In order to account for strong correlations, we applied the DFT+U method with fixed Hubbard U of 4.5 eV. This parameter describes the on-site Coulomb repulsion between f electrons and its value has been derived from spectroscopic data.[10] DFT+U has been used successfully in many previous computational studies of uranium-containing compounds.[11] We used the plane-wave, periodic quantum-espresso code[12] and PBE and PBEsol exchange−correlation functionals,[13] which are known to provide good equilibrium structures, even for uranium compounds.[14] Two different DFT functionals and the DFT+U method have been applied in order to better constrain the calculated structures and energies. The crystalline solids were treated as continuous in all three spatial dimensions by applying periodic boundary conditions. The supercells of both α- and β-$Ba_2[UO_2(PO_4)_2]$ contained 30 atoms (two formula units). We applied an energy cutoff of 60 Ryd, and 2 × 3 × 3 Methfessel−Paxton k-point grids,[15] resulting in 10 k-points for the α structure and 8 k-points for the β structure, which was sufficient to provide energy convergence within 0.025 kJ/mol pfu (per formula unit). We performed two kinds of calculations: (1) fixing the lattice parameters to the ones determined experimentally and reported in Table 1 and (2) relaxing the lattice parameters to a given pressure. In both calculations the ionic configurations were relaxed to the equilibrium positions, so that the maximum component of the residual forces on the ions was less than 0.005 eV/Å. The fixed-pressure calculations were performed by relaxing the lattice parameters and ionic positions so that the resulting pressure was 0 GPa with a tolerance of 0.01 GPa. The core electrons of the computed atoms were replaced by ultrasoft pseudopotentials[16] and the $2s^2\ 2p^4$ electrons of oxygen and $6s^2\ 6p^6\ 5f^3\ 6d^1\ 7s^2$ electrons of uranium were treated explicitly. The vibrational frequencies used to estimate the free energies were computed with density functional perturbation theory and PBEsol exchange−correlation functional as implemented in the quantum-espresso code.

3. RESULTS AND DISCUSSION

3.1. H_3BO_3/B_2O_3 Flux as a Reaction Medium for the Preparation of New Uranium Compounds. H_3BO_3/B_2O_3 fluxes have been widely used to prepare borate compounds[17] and have been employed here, too. H_3BO_3 decomposes at high temperatures to form B_2O_3. Therefore, in the present study with synthesis temperatures of 1000 or 1300 °C, the actual flux material was B_2O_3. From 1987 to 1991, Gasperin and co-workers[18] synthesized several actinide (U, Th) borates by use of B_2O_3 flux at high temperatures (1080−1200 °C). Recently, Wang et al.[19a−m] and Polinski et al.[19n,o] expanded the knowledge of the actinide borate family by using H_3BO_3 flux at much lower temperatures (190−240 °C). It is worth noting that, in these syntheses, borate was incorporated into the structures as the major ligand. In the present work, despite the fact that all the compounds were synthesized in the presence of H_3BO_3 or B_2O_3, no borate was incorporated into the structure under the experimental conditions used. In the course of our previous study, it was found that a pure uranyl borate, β-$UO_2B_2O_4$,[19g] is easily formed at high temperatures (up to 1200 °C) despite the presence of other anions in the system. It is interesting to note how changing experimental parameters are able to direct the phase formation. With the same molar ratios as for the preparation of **2**, but using a lower temperature of 1000 °C instead of 1300 °C, we obtained the complex nanostructured $Ba_5[(UO_2)(PO_4)_3(B_5O_9)]\cdot nH_2O$ (BaBPU1).[20] Therefore, we suppose that **2** forms following the thermal decomposition of BaBPU1. In the arsenate system we have not found any mixed B/As phases and only compound **3** formed in the reactions.

3.2. Structure of α-$Ba_2[UO_2(PO_4)_2]$ (1) and Distortion of Uranium Coordination. A fragment of the crystal structure of **1** is shown in Figure 1a. Atomic positions and displacement parameters are given in Table S1 in Supporting Information. The structure contains one symmetrically independent U, two Ba, and two P atoms. It is based on infinite 1D chains with a cation topology shown in Figure 1c. A ball-and stick representation of one of these chains is shown in Figure 2. The chains are composed of UO_7 pentagonal bipyramids and PO_4 tetrahedra. Each UO_7 polyhedron is connected to three PO_4 tetrahedra by corner-sharing and to one PO_4 tetrahedron by edge-sharing (Figures 1c and 3a). The uranyl polyhedra are isolated from each other, as are the phosphate tetrahedra. $P(1)O_4$ is connected to uranyl polyhedra only by corner-sharing, whereas $P(2)O_4$ is connected to uranyl polyhedra via both corner-sharing and edge-

dx.doi.org/10.1021/ic500965v | Inorg. Chem. 2014, 53, 7650−7660

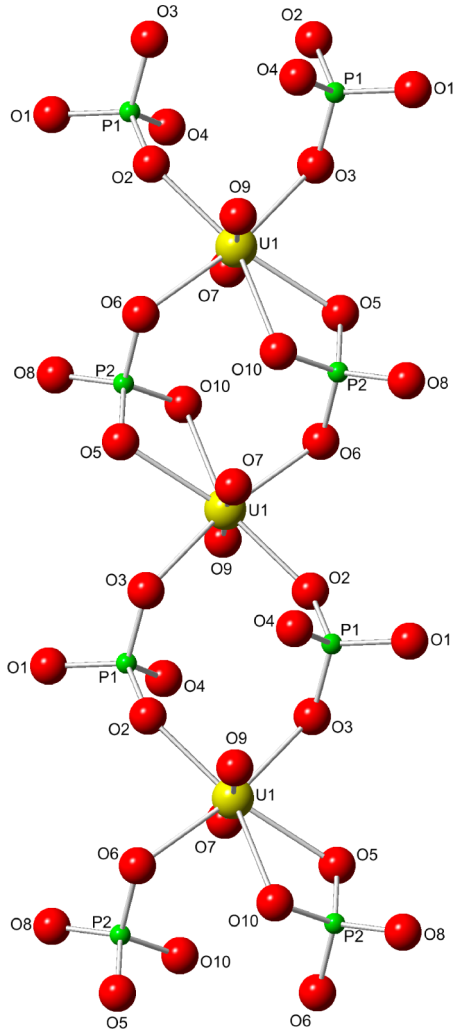

Figure 2. Ball-and-stick view of uranyl phosphate chain in **1**. U is shown in yellow, P in green, and O in red.

sharing (Figures 1c and 2). Similar coordination has been reported earlier for isolated $UO_2(SO_4)_4^{6-}$ clusters (Figure S2, Supporting Information);[21,22] however, **1** is the first uranium compound with an infinite chain that exhibits such mixed coordination. Note that rings R1 [UO_7−P(2)O_4−UO_7−P(2)-O_4] and R2 [UO_7−P(1)O_4−UO_7−P(1)O_4] alternate along the chain direction. The Ba atoms are located in the space between the uranyl phosphate chains.

At 1.770(1) Å, the U═O_{Ur} bond lengths of UO_2^{2+} are in the expected range. By way of contrast, the O_{Ur}═U═O_{Ur} bond angle [173.67(4)°] (Table S3, Supporting Information) is rather unusual and indicates that the normally fairly linear, rod-shaped uranyl ion is significantly bent (Figure 3c). Three of the equatorial bonds are relatively short (around 2.30 Å) and belong to O_{eq} atoms O(2), O(3), and O(6), which link uranyl and phosphate polyhedra via common corners. Two longer bonds involve O_{eq} atoms in the shared edge, viz., O(5) [2.430(1) Å] and O(10) [2.749 (2) Å] (Table 2). The O_{eq}−U═O_{Ur} angles deviate significantly from the normally found approximately 90°; in particular, O_{eq}(10)−U(1)═O_{Ur}(9), with its value of 70.15(5)°, is much lower compared to others (Table S3, Supporting Information). The remarkable geometrical features of O(10) are the consequence of the particular orientation of the edge-sharing P(2)O_4 tetrahedron with respect to the UO_2^{2+}. Usually shared edges, if any, between uranyl bipyramids and tetrahedral groups are more or less perpendicular to the UO_2^{2+} axis. In **1**, however, the bidentate P(2)O_4 group is tilted by approximately 45° relative to UO_2^{2+} (Figures 2 and 3a). A least-squares plane calculated for the O_{eq} atoms O(2), O(3), O(5), and O(6) shows that these atoms define a fairly flat plane with deviations from the plane on the order of 0.05 Å. However, O(10) has a distance of about 1.5 Å from this plane (see Table S4 in Supporting Information). This is of the same order of magnitude as the deviations of the apical O_{Ur} atoms O(7) (−1.61 Å) and O(9) (1.89 Å). Each ring, R1 and R2, transforms under the action of an inversion at its center relating two opposite UO_7 bipyramids and P(2)O_4 or P(1)O_4 tetrahedra, respectively. If we now consider ring R1, we find that triples O(10)−O(9)−O(7) and inversion-

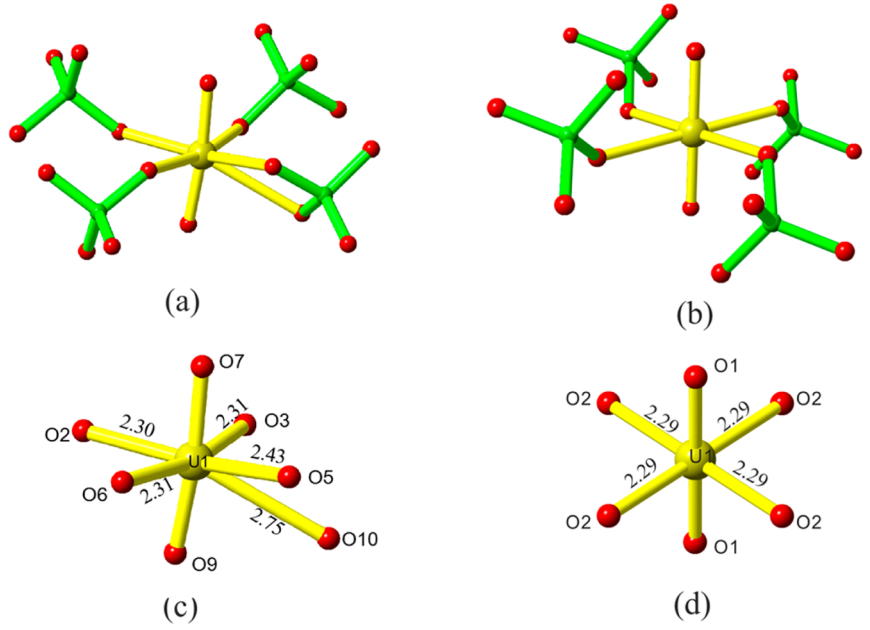

Figure 3. Uranium coordination in (a, c) **1** and (b, d) **2**. U is shown in yellow, P in green, and O in red.

dx.doi.org/10.1021/ic500965v | *Inorg. Chem.* 2014, 53, 7650−7660

Table 2. Selected Bond Distances for 1 and 2

bond	distance, Å	bond	distance, Å
	α-$Ba_2[UO_2(PO_4)_2]$ (**1**)		
U(1)−O(2)	2.297(1)	P(1)−O(1)	1.524(1)
U(1)−O(3)	2.308(1)	P(1)−O(2)	1.557(1)
U(1)−O(5)	2.430(1)	P(1)−O(3)	1.559(1)
U(1)−O(6)	2.314(1)	P(1)−O(4)	1.510(1)
U(1)═O(7)	1.771(1)	P(2)−O(5)	1.548(1)
U(1)═O(9)	1.770(1)	P(2)−O(6)	1.554(1)
U(1)−O(10)	2.749(2)	P(2)−O(8)	1.510(1)
		P(2)−O(10)	1.524(1)
Ba(1)−O(4)	2.697(1)	Ba(2)−O(4)	2.631(1)
Ba(1)−O(10)	2.760(1)	Ba(2)−O(8)	2.671(1)
Ba(1)−O(1)	2.828(2)	Ba(2)−O(5)	2.790(2)
Ba(1)−O(8)	2.863(1)	Ba(2)−O(1)	2.841(1)
Ba(1)−O(6)	2.920(1)	Ba(2)−O(2)	2.924(1)
Ba(1)−O(6)	2.924(1)	Ba(2)−O(3)	2.960(1)
Ba(1)−O(7)	2.934(1)	Ba(2)−O(3)	2.999(1)
Ba(1)−O(5)	2.936(1)	Ba(2)−O(9)	3.070(1)
Ba(1)−O(1)	2.947(1)	Ba(2)−O(10)	3.264(2)
Ba(1)−O(2)	23.002(2)		
	β-$Ba_2[UO_2(PO_4)_2]$ (**2**)		
U(1)═O(1) × 2	1.787(9)	P(1)−O(3)	1.497(7)
U(1)−O(2) × 4	2.294(6)	P(1)−O(4)	1.526(8)
Ba(1)−O(1) × 2	3.230(5)	P(1)−O(2) × 2	1.538(6)
Ba(1)−O(4)	2.667(8)	Ba(1)−O(2) × 2	2.948(6)
Ba(1)−O(4)	2.755(10)	Ba(1)−O(2)# × 2	2.952(6)
Ba(1)−O(3)	2.820(8)	Ba(1)−O(3)# × 2	2.986(3)

related O(10)*−O(9)*−O(7)* lie on opposite sides of the least-squares planes with similar distances ±1.5−1.9 Å. This brings O(10) and O(10)* into close contact with the O_{Ur} on their respective side of the equatorial plane with distances O(10)−O(9) = 2.72 Å and O(10)−O(7) = 2.80 Å. Note that, for a given O(10) or O(10)*, the partners [O(9) and O(7) or O(9)* and O(7)*, respectively] belong to opposite UO_7 bipyramids in R1. Let us restrict to the case of O(9) and its contact with O(10) and, for the sake of argument, let us suppose that the uranyl ion in the UO_7 bipyramid was ideally linear. In this case O(9) had to take the position O(9′), provided all other oxygens were fixed (Figure 4). Then, however, the distance

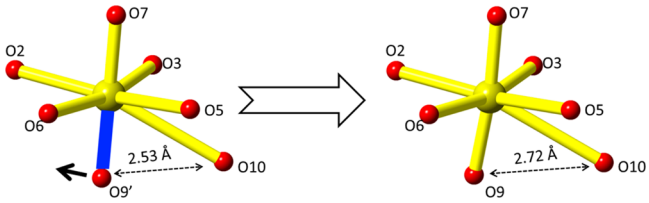

Figure 4. Cartoon showing the proposed steric hindrance between O(10) and O(9)′ in **1** (left) and its release (right-hand side). A similar interaction occurs between O(7) and a symmetry-related O(10) (not shown). The combined interaction leads to the observed bending of the uranyl cation with an angle O(9)═U═O(7) of about 173°. U is shown in yellow and O in red.

O(9′)−O(10) would be 2.53 Å, which is too short for normal nonbonded O−O distances. (Note that distances between oxygens in the same, rather rigid, PO_4 tetrahedra are not considered here.) Therefore, repulsive forces could be expected that push O(9′) away from O(10) into the position of O(9), resulting in the actually observed longer distance of 2.72 Å between O(9) and O(10) (Figure 4). This increased distance can be considered to result in an energy gain (cf. Figure 4).[22] A similar argument applies for the interaction between O(10) and O(7). As O(9) and O(7) on one side of the least-squares planes belong to two opposite UO_7 bipyramids, the respective repulsions emanating from O(10) act in opposite directions, and because of the inversion symmetry, these oppositely oriented repulsions occur also on the other side of the equatorial planes, and as a result, the uranyl ions are bent away from O(10) and O(10)*, such that the angle O(7)═U(1)═O(9) becomes the observed 173.67(4)° (Table S3, Supporting Information).

The O−P−O angles are in the range from 104.83(7)° to 114.04(7)°, with the largest one occurring at the shared edge of $P(2)O_4$. This stretching can be supposed to be due to the described repulsive interactions between oxygens at the shared edge and the apical uranyl oxygens. The P−O bond lengths range from 1.510(1) to 1.559(1) Å in $P(1)O_4$ and from 1.510(1) to 1.554(1) Å in $P(2)O_4$ (Table 2).

Ba(1) and Ba(2) are coordinated by 10 or 9 oxygens, respectively, whereby each one contains one O_{Ur} in its coordination sphere. The Ba−O bond distances range from 2.697(1) to 3.001(2) Å in Ba(1) and from 2.631(1) to 3.264(2) Å in Ba(2), where the latter value pertains to Ba(2)−O(10). The bond valence sums (BVS) are 5.91 for U(1)[23] and 4.80, 4.84, 2.09, and 1.92, for P(1), P(2), Ba(1), and Ba(2), respectively (Table S5, Supporting Information).[24]

It is instructive to consider in slightly more detail the situation around the two symmetrically independent PO_4 tetrahedra and their bonding. Both tetrahedra are related by a $t/2$ pseudotranslation along the chain (see Figure 2), where t is the chain periodicity. $P(1)O_4$ contains the oxygen atoms O(1), O(2), O(3), and O(4), and $P(2)O_4$ contains atoms O(5), O(6), O(8), and O(10). Pairs of pseudotranslationally related O atoms can be distinguished, viz., O(1)/O(8), O(3)/O(6), O(2)/O(5), and with some reservation, O(4)/O(10). O(1) and O(8) make two bonds with Ba atoms, in addition to the bond with the respective P; O(3) and O(6) are bound with two Ba, one P, and one U. O(2) and O(5) are also bound with two Ba, one P, and one U, whereby O(5)−U (2.43 Å) is considerably longer than O(2)−U (2.30 Å). If the two PO_4 tetrahedra were equivalent, then O(4) and O(10) should have the same coordination. However, O(4) is similar to O(1) and O(8) in that it forms two bonds with Ba in addition to its bond with P(1), but O(10) diverges sharply. It makes a short bond with P(2), as expected, but only one short bond with Ba (2.76 Å) and its uncommon bond with U of 2.75 Å. The second Ba is at a distance of 3.26 Å, which is at the limit of what may be accepted as a bond. Disregarding its bond with U, O(10) would be severely underbonded [about 1.5 valence units (vu); for bond valences see Table S5 in Supporting Information] and this might be the reason why O(10) tries to make some "good" distance from the uranyl group, even at the expense of a distortion of the latter. The bond U−O(10) adds about 0.25 vu to the BVS of O(10) (1.84) and the long bond U−Ba(2) adds another 0.07; thus it seems that O(10) can still be considered as underbonded. This lends itself to the speculation that some contribution to the BVS of O(10) stems from the interaction between O(10) and the O_{Ur} atoms O(9) and O(7) as described above. The contributions of the "real" O_{eq} atoms O(2), O(3), and O(6) to the BVS of U(1) are about 0.6 each; O(5) has to share its contribution with O(10) (0.25 vu) and donates only 0.46 vu. Each O_{Ur} donates about 1.7 vu to the BVS of U, a value that is not significantly different from what is observed in **2** (see below).

dx.doi.org/10.1021/ic500965v | Inorg. Chem. 2014, 53, 7650−7660

Table 3. Crystallographic Data for 1 and 2

	α-$Ba_2[UO_2(PO_4)_2]$ (1)					β-$Ba_2[UO_2(PO_4)_2]$ (2)				
		calcd[a]					calcd[a]			
	exptl	PBE	PBE+U	PBEsol	PBEsol+U	exptl	PBE	PBE+U	PBEsol	PBEsol+U
a (Å)	6.774(2)	6.651	6.733	6.558	6.623	12.6020(9)	12.510	12.549	12.347	12.372
b (Å)	8.634(3)	8.739	8.694	8.508	8.427	5.3875(4)	5.536	5.637	5.441	5.538
c (Å)	9.030(4)	9.321	9.255	9.159	9.100	6.9527(3)	7.103	6.963	6.875	6.791
α (deg)	104.55(3)	105.884	104.147	105.070	103.001					
β (deg)	93.87(2)	95.275	95.140	95.131	94.087	102.621(4)	103.111	103.294	103.386	103.618
γ (deg)	112.13(3)	108.752	110.571	109.254	111.442					
V (Å^3)	465.7(3)	484.558	483.573	457.889	454.1184	460.64(5)	479.077	479.310	449.299	452.284

[a]Data were derived by DFT and DFT+U methods with relaxation of lattice parameters to P = 0 GPa at T = 0 K. The four calculated numbers represent results obtained with PBE, PBE+U, PBEsol, and PBEsol+U methods.

Table 4. Selected Bond Distances for 1 and 2 Computed by DFT Methods

	calcd distance[a] (Å)					calcd distance[a] (Å)			
bond	PBE	PBE+U	PBEsol	PBEsol+U	bond	PBE	PBE+U	PBEsol	PBEsol+U
					α-$Ba_2[UO_2(PO_4)_2]$ (1)				
U(1)−O(2)	2.311	2.353	2.286	2.327	P(1)−O(1)	1.546	1.547	1.543	1.543
U(1)−O(3)	2.331	2.392	2.303	2.361	P(1)−O(2)	1.534	1.540	1.577	1.575
U(1)−O(5)	2.502	2.571	2.469	2.528	P(1)−O(3)	1.588	1.586	1.588	1.585
U(1)−O(6)	2.316	2.383	2.288	2.353	P(1)−O(4)	1.534	1.540	1.532	1.538
U(1)═O(7)	1.833	1.794	1.826	1.788	P(2)−O(5)	1.572	1.572	1.572	1.572
U(1)═O(9)	1.826	1.788	1.818	1.778	P(2)−O(6)	1.585	1.585	1.584	1.584
U(1)═O(10)	2.517	2.593	2.479	2.582	P(2)−O(8)	1.531	1.539	1.529	1.537
					P(2)−O(10)	1.561	1.561	1.560	1.556
					β-$Ba_2[UO_2(PO_4)_2]$ (2)				
U(1)−O(1)	1.815	1.784	1.806	1.776	P(1)−O(3)	1.535	1.538	1.532	1.536
U(1)−O(2)	2.309	2.367	2.288	2.342	P(1)−O(4)	1.539	1.544	1.538	1.542
					P(1)−O(2)	1.586	1.584	1.585	1.582

[a]The four numbers represent results obtained with PBE, PBE+U, PBEsol, and PBEsol+U methods.

It is interesting to compare the described situation around O(10) with that of the pseudotranslationally related O(4) in ring R2. The distances O(4)−O(7) and O(4)−O(9) are 3.12 and 2.97 Å, respectively. Bond valences for O(4) are −1.29 from P(1), −0.33 from Ba(1), and −0.40 from Ba(2), giving a BVS of −2.02 (Table S5, Supporting Information). This demonstrates that O(4) is, indeed, well-behaved.

3.3. Structure of β-$Ba_2[UO_2(PO_4)_2]$ (2). The situation in **2** appears to be simpler. A fragment of its crystal structure is shown in Figure 1b. It is based on 1D chains parallel to the *b* axis. The structure of the chains and their cationic topology in the form of two-dimensional (2D) black and white graphs are shown in Figure 1d. The chains are based on UO_6 square bipyramids and PO_4 tetrahedra. Each equatorial oxygen atom in the UO_6 square bipyramid is corner-connected with a PO_4 tetrahedron; thus one UO_6 square bipyramid is connected to four phosphate tetrahedra, and vice versa (Figures 1d and 3b). The PO_4 tetrahedra on each side of the chain are related by inversion. This is topologically the same situation as in **1**, where, however, we have the described extra bonding and subsequent distortion. The Ba atoms reside in the space between uranyl phosphate chains and are coordinated by 11 oxygen atoms.

In contrast to **1**, the square bipyramid in **2** appears to be well-behaved with U═O_{Ur} bond distances between 1.787(9) and 2.294(6)Å for all U−O_{eq} distances in the equatorial plane (Figure 3d, Table 2). The angle O_{Ur}═U═O_{Ur} is 180°, by symmetry. The angles O_{eq}−U═O_{Ur}, however, are not 90°, as could have been expected for a perfect bipyramid, but deviate by 4.7° from this value in such a way that the O_{Ur} atoms at opposite apexes of the uranyl cation are tilted in opposite directions, without changing the angle O_{Ur}═U═ O_{Ur} from 180° (Table S3, Supporting Information). This is the effect of a putative repulsive interaction between O(4) of the PO_4 tetrahedra and the apical O(1), similar to the situation described for **1**, resulting in a distance of about 2.90 Å. The difference is here that the interactions on opposite sides of the uranyl group are directed into opposite directions. In **1** the interaction was in the same direction, which resulted in bending of the uranyl group, while here it is directed in the opposite direction, resulting in the tilting. P−O bond distances are quite normal and range from 1.497(7) to 1.538(6) Å with O−P−O angles from 105.5(4)° to 110.6(3)°. BVS are 5.74 for U[23] and 4.96 for P.[24] The coordination number (11) of barium is greater than in **1** (see above).[25] The Ba−O bond distances range from 2.666(9) to 3.230(5) Å, which results in a bond valence sum of 2.02 for Ba(1) in **2** (Table S5, Supporting Information).[24]

3.4. Computational Study of $Ba_2[UO_2(PO_4)_2]$ Polymorphs. At first glance, one might think intuitively that the energy needed to distort the uranyl bipyramid and the phosphate tetrahedron in the structure of **1** would penalize this phase in favor of **2**. Experimentally, however, only **1** could be obtained as a pure phase under various conditions, and even a heat treatment at 1000 °C for 24 h did not change it. Therefore, it was interesting to get some deeper insight into the relative stabilities of **1** and **2**. In order to achieve this goal, a set of DFT and DFT+U calculations with PBE and PBEsol exchange−correlation func-

dx.doi.org/10.1021/ic500965v | Inorg. Chem. 2014, 53, 7650−7660

Table 5. Total Energies E and Free Energies F of $Ba_2[UO_2(PO_4)_2]$ Phases Computed by Different DFT Methods[a]

	PBE		PBE+U		PBEsol		PBEsol+U			ST (kJ/mol)	
phase	E(kJ/mol)	F(kJ/mol)	E(kJ/mol)	F(kJ/mol)	E(kJ/mol)	F(kJ/mol)	E(kJ/mol)	F(kJ/mol)	ZPE (kJ/mol)	at 300 K	at 1000K
α	0		0		0		0		8.5	140.4	206.2
α (relaxed)	0		0		0		0		8.5	140.4	206.2
β	16.7	13.4	9.6	6.3	20.2	16.9	12.8	9.5	8.4	144.4	209.4
β (relaxed)	16.9	13.6	3.7	0.4	23.6	20.3	9.8	6.5	8.4	144.4	209.4

[a]α-Phase is taken as a reference. The last three columns indicate zero-point energy (ZPE) and computed vibrational entropy at T = 300 K and 1000 K. Free energy is computed according to $F = E - TS$ (T = 1000 K). The contribution from change in volume at ambient condition is below 0.1 kJ/mol and therefore is not considered here.

tionals was performed. It is well-known that, of the two chosen functionals, PBEsol results in better structural parameters while PBE gives better energies. We will therefore elaborate on the performance of these functionals for the prediction of structural properties of the measured polymorphs. This will allow us to better assess the energy differences between the two materials.

First, we compared the lattice parameters derived with the aforementioned methods under the assumption that P = 0 GPa and T = 0 K. The results are given in Table 3. In terms of volume, the PBE functional overestimates its value by up to 4%, which is a well-known property of this functional,[26] while PBEsol underestimates it by up to 3%. Regarding the individual lattice parameters, the PBEsol functional-derived results match the experimental numbers better in most cases. Therefore, for further discussion we will use results obtained with the PBEsol +U method. Although neither method gives superior prediction of the individual lattice parameters, because the PBEsol functional-based methods slightly better reproduce the experimental volumes, in further discussion we will use results obtained with the PBEsol+U method.

*3.4.1. α-$Ba_2[UO_2(PO_4)_2]$ (**1**).* Selected bond lengths obtained from DFT and DFT+U calculations are reported in Table 4. The PBEsol+U equilibrium structure results in almost the same values obtained from the diffraction experiment, namely, U═O_{Ur} bond lengths for UO_2^{2+} range from 1.778 to1.788 Å, and the O_{Ur}═U═O_{Ur} angle of 174.5° shows the same distortion as found experimentally. The distances between uranium and O_{eq} are from 2.327 to2.582 Å, with U(1)−O(2) being 0.03 Å longer and U(1)−O(10) 0.167 Å shorter than the values reported in Table 2, although the average of these two bonds agrees well (within 0.04 Å) with experiment. Interestingly, DFT+U significantly outperforms DFT in this aspect, with PBEsol giving an average of these bonds that is 0.12 Å shorter. The O(9)═U(1)−O(10) angle is 75.2° and only slightly larger than the measured value. It is particularly satisfying to see that the experimentally observed long distances for U(1)−O(5) (2.43 Å) and U(1)−O(10) (2.75 Å) are well reproduced by the computational approach. The same is true for the critical O(9)−O(10) distance (computed 2.74 Å, measured 2.72 Å).

The P−O bond lengths range from 1.538 to 1.585 Å. These bond lengths are ∼0.03 Å longer than the measured values. However, such an overestimation of P−O bond length is a common feature of DFT functionals.[27] On the other hand, the O−P−O angles range from 104.7° to 114.2° which is again in excellent agreement with the experimental structure.

*3.4.2. β-$Ba_2[UO_2(PO_4)_2]$ (**2**).* The computed DFT structure of β phase is in excellent agreement with the measured structure parameters. The U═O bond in the uranyl group is 1.776 Å, which is almost the same as the measured value, and the computed U−O distance of 2.342 Å in the equatorial plane is only slightly larger than the measured values of 2.294 Å (Tables 2 and 4). The O_{eq}−U═O_{Ur} angle is 85.6°, which is in excellent agreement with the measured value. Similar to α-$Ba_2[UO_2(PO_4)_2]$, the computed P−O distances in β-$Ba_2[UO_2(PO_4)_2]$ are ∼0.04 Å longer than the measured bond lengths, while the O−P−O angles range from 104.3° to 112.0°, which show good consistency with the experimental data.

3.4.3. Comparison between α- and β-$Ba_2[UO_2(PO_4)_2]$. In Table 5, the energies and free energy differences between the two polymorphs are reported. With DFT calculations, it was found that the difference in energy between the α- and β-phases ranges from 9.6 to 20.2 kJ/mol pfu depending on the computational method, indicating the α-$Ba_2[UO_2(PO_4)_2]$ phase is energetically favored. Upon relaxation of the lattice parameters to P =0 GPa, the energy difference is slightly different, ranging from 3.7 to 23.6 kJ/mol pfu. When one considers the free energy instead, also all the applied methods predict the α-$Ba_2[UO_2(PO_4)_2]$ phase to be more stable than β-$Ba_2[UO_2(PO_4)_2]$. It is known that, because of bad handling of systems containing strongly correlated d and f electrons, DFT energies can carry significant error. PBE functional also results in a large error (∼60 kJ/mol) for the atomization energies[26] and enthalpies of reactions involving U-bearing molecules.[28] For example, for uranium fluorides, oxides, and oxofluorides, it overestimates the reaction enthalpies by as much as 50%.[14] We note that the investigated structures of α- and β-$Ba_2[UO_2(PO_4)_2]$ are rather similar, with α being a distorted version of β, and only significant differences between their electronic structures could lead to a significant error in the derived energy difference. In order to search for potential differences in the electronic structures of the two considered phases, we performed a Loewdin population analysis of the charge distribution between different atomic orbitals. The result is given in Table 6. The occupations projected on the atomic orbitals are very similar in both cases, which indicate very similar electronic structures of the two phases.

Table 6. Loewdin Population Analysis of U Atoms in 1 and 2

	n (6s)	n (6p)	n (6d)	n (5f)
α-$Ba_2[UO_2(PO_4)_2]$ (**1**)	2.18	5.69	2.44	2.87
β-$Ba_2[UO_2(PO_4)_2]$ (**2**)	2.18	5.68	2.43	2.90

We also compare the electronic density of states computed for the two structures (Figure 5). The results are also very similar in terms of the energies and shapes, which shows that the two phases indeed have very similar electronic structure. The only difference is a peak between −6 and −5 eV, which is of lower energy by 0.33 eV in the case of the α polymorph. The analysis of partial densities of states shows that in both polymorphs this peak arises mainly from 2s and 2p orbitals of the oxygens of UO_2^{2+}. In the case of α-phase, the energy of these orbitals is lowered because of the decrease in O(9)−O(10) (2.74 Å) and O(7)−

dx.doi.org/10.1021/ic500965v | Inorg. Chem. 2014, 53, 7650−7660

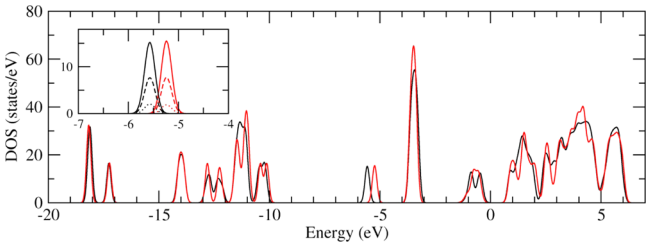

Figure 5. Electronic density of states (DOS) for α- (black) and β- (red) $Ba_2[UO_2(PO_4)_2]$ computed with PBEsol+U method. (Inset) Contributions to the −5.5 eV peaks from 2s (dashed line) and 2p (dotted line) states of O(7) and O(9) atoms in case α and O(1) atom in case β.

O(5) (2.75 Å) bond lengths compared with O(1)−O(2) (2.83 Å) in the β-phase. This seems to result in more attractive interaction between the oxygen atoms involved and makes the α polymorph more stable.

We note that both PBE+U and PBEsol+U calculations, which by correcting for strong correlations should give more reliable energies, resulted in smaller energy differences between α and β polymorphs than PBE and PBEsol functionals. Nevertheless, all the applied methods give lower energies for the α-phase and thus predict that it is more stable than the β-phase. This seems to be in accordance with the laboratory experiments.

3.5. Structure of $Ba_2[UO_2(AsO_4)_2]$ (3). A fragment of the crystal structure of **3** is shown in Figure 6a. This structure contains $[UO_2(AsO_4)_2]^{4-}$ 2D layers and Ba atoms residing between the layers. There are two similar coordinated U sites and four As sites in **3**. The layers are based upon UO_6 square bipyramids and AsO_4 tetrahedra. Each UO_6 square bipyramid connects to four AsO_4 tetrahedra via corner-sharing to form a $[UO_2(AsO_4)_4]$ cluster, and each AsO_4 tetrahedron is shared with two UO_6 square bipyramids. Every two $[UO_2(AsO_4)_4]$ clusters connect to each other via sharing two AsO_4 tetrahedra to form a $[(UO_2)_2(AsO_4)_6]$ block, which is the fundamental building block (FBB) of **3**. Each FBB is connected to another four FBBs through sharing the corner AsO_4 tetrahedra, resulting in a herringbone-type pattern of the FBBs. On each side of the FBBs, the AsO_4 tetrahedra in the FBBs point in the same direction. An alternative description of the structure of **3** is that six UO_6 tetragonal bipyramids and six AsO_4 tetrahedra are linked together to form a 12-membered oblong ring (Figure 6b). The cationic topology is shown in Figure 6c and is similar to some known structures.[29] However, despite the topological identity with known phases, one has to note that the uranium environment in **3** is a square bipyramid UO_6, whereas in all previously described phases with the same topology there are pentagonal bipyramids UO_7.

The U−O bond distances are quite normal in **3**, from 1.771(3) to 1.802(3) Å for bonds within UO_2^{2+} ion and from 2.253(3) to 2.323(3) Å for U−O_{eq} bonds (Table 7). Note that the angle O_{Ur}═U(1)═O_{Ur} is around 180° by symmetry, whereas O_{Ur}═U(2)═O_{Ur} is 176° (Table S3, Supporting Information), thus indicating that this uranyl group is also bent, although to a lesser extent than in **1**. The bond valence sums for U(1) and U(2) are 5.71 and 5.82, respectively.[23] The As−O bonds ranges from 1.660(3) to 1.715(3) Å in AsO_4 tetrahedra with bond valence sums of 4.96, 4.95, 5.00, and 5.01 for As(1), As(2), As(3), and As(4) sites, respectively (Table S6, Supporting Information).[24]

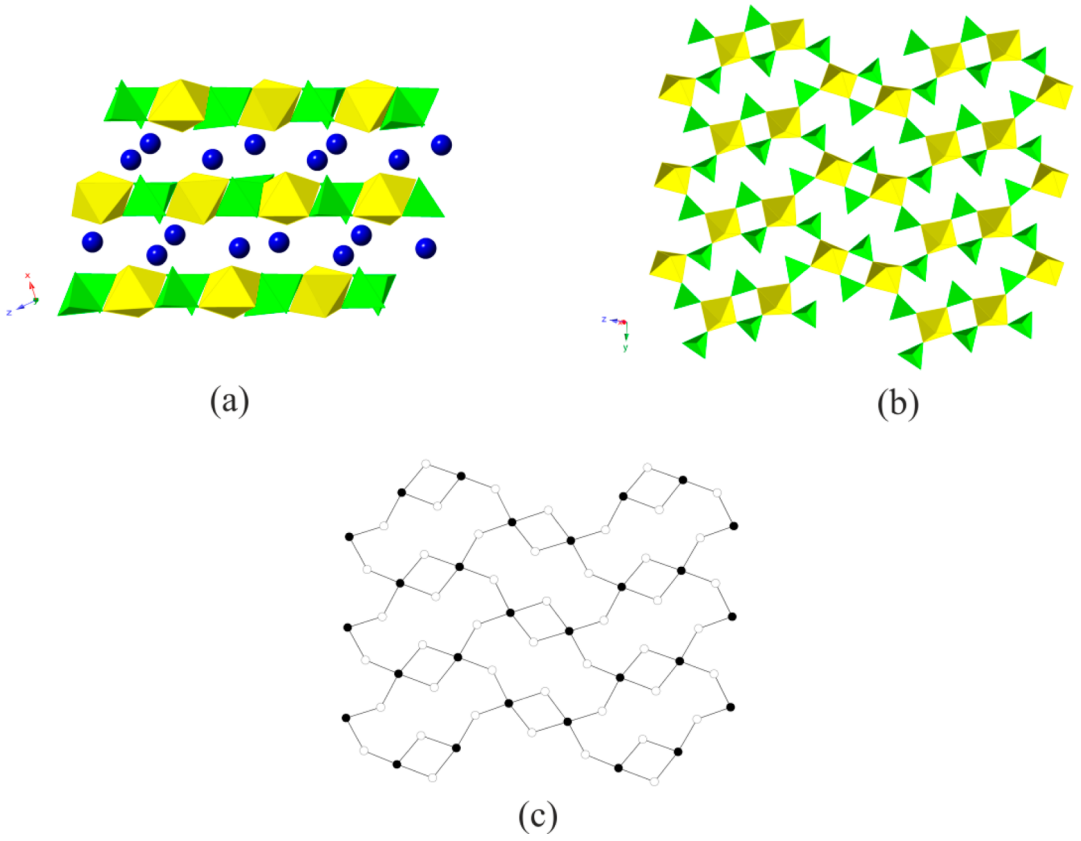

Figure 6. (a, b) Polyhedral representation of the crystal structure of **3** and (c) its topological representation. Uranium and phosphorus polyhedra are shown in yellow and green, respectively, and blue spheres stand for Ba atoms.

dx.doi.org/10.1021/ic500965v | Inorg. Chem. 2014, 53, 7650−7660

Table 7. Selected Bond Distances for $Ba_2[UO_2(AsO_4)_2]$ (3)

bond	distance (Å)	bond	distance (Å)
U(1)═O(17)	1.786(3)	As(1)−O(4)	1.660(3)
U(1)═O(9)	1.792(3)	As(1)−O(13)	1.666(3)
U(1)−O(20)	2.253(3)	As(1)−O(6)	1.712(3)
U(1)−O(1)	2.295(3)	As(1)−O(1)	1.714(3)
U(1)−O(16)	2.320(3)	As(2)−O(7)	1.661(3)
U(1)−O(2)	2.323(3)	As(2)−O(5)	1.669(3)
U(2)−O(14)	1.771(3)	As(2)−O(2)	1.710(3)
U(2)−O(8)	1.802(3)	As(2)−O(3)	1.715(3)
U(2)−O(10)	2.256(3)	As(3)−O(18)	1.658(3)
U(2)−O(12)	2.268(3)	As(3)−O(15)	1.672(3)
U(2)−O(6)	2.281(3)	As(3)−O(20)	1.695(3)
U(2)−O(3)	2.308(3)	As(3)−O(12)	1.714(3)
		As(4)−O(11)	1.670(3)
		As(4)−O(19)	1.673(3)
Ba(1)−O(7)	2.622(3)	As(4)−O(10)	1.692(3)
Ba(1)−O(7)	2.718(3)	As(4)−O(16)	1.702(3)
Ba(1)−O(19)	2.873(4)	Ba(3)−O(4)	2.645(3)
Ba(1)−O(6)	2.892(3)	Ba(3)−O(18)	2.702(4)
Ba(1)−O(13)	2.912(3)	Ba(3)−O(4)	2.705(3)
Ba(1)−O(6)	2.935(3)	Ba(3)−O(5)	2.784(3)
Ba(1)−O(10)	3.039(4)	Ba(3)−O(3)	2.857(3)
Ba(1)−O(5)	3.048(3)	Ba(3)−O(2)	2.910(3)
Ba(1)−O(1)	3.128(3)	Ba(3)−O(2)	3.034(3)
Ba(1)−O(8)	3.194(4)	Ba(3)−O(13)	3.250(3)
Ba(2)−O(15)	2.639(3)	Ba(4)−O(11)	2.652(3)
Ba(2)−O(15)	2.678(3)	Ba(4)−O(11)	2.661(3)
Ba(2)−O(19)	2.760(3)	Ba(4)−O(18)	2.771(3)
Ba(2)−O(13)	2.874(3)	Ba(4)−O(12)	2.876(3)
Ba(2)−O(16)	2.875(3)	Ba(4)−O(9)	2.884(3)
Ba(2)−O(1)	2.934(3)	Ba(4)−O(3)	2.984(3)
Ba(2)−O(8)	2.972(3)	Ba(4)−O(5)	3.010(4)
Ba(2)−O(17)	3.143(4)	Ba(4)−O(20)	3.287(4)

3.6. Structural Relationship in the $Ba_2[UO_2(TO_4)_2]$ (T = P, As) Family. As noticed previously, **1** and **2** are polymorphic structures, the only difference being that one out of four phosphate tetrahedral surrounding the uranyl group is edge-connected. Thus, conceptually **1** can be transformed into **2** by cutting the longest U−O bond in **1** with subsequent readjustment of bond lengths and angles. A reverse procedure would transform **2** into **1**.

The same chain topology as in the structure of **2** has been found in several other compounds containing uranyl square bipyramids corner-linked with TO_4 tetrahedra (T = P, Mo, As). Polyhedral representations of these chains are given in Figure S3 in Supporting Information. They demonstrate the highly variable geometry of these chains due to the flexible corner linkage between uranyl group and the corresponding TO_4 tetrahedra. With due reservation, the chain occurring in **1** could also be included in this series, however, as an extreme case.

The structural relationship between such 1D chains and the 2D layers in **3** is quite interesting and lends itself to a speculation whether a modular approach might be possible to explain the relationships between chain and layer types of this kind of compounds. This approach is illustrated by the structural relationships between **2** and **3** as shown in Figure 7a, where a chain of **2** is shown and blocks $[(UO_2)_2(TO_4)_6]$ (group A, red dashed outline) and $[(UO_2)_2(TO_4)_2]$ (group B, blue dashed outline) are emphasized. When the chain is cut appropriately (arrows), group B rotated by 180° as shown by the red arrow in Figure 7a, and the pieces joint together periodically, then the zigzag chains of Figure 7b are obtained. When finally neighboring zigzag chains are connected as indicated by green arrows in Figure 7b, the layer shown in Figure 7c is obtained, which is, of course, identical with the 2D layer of **3** (cf. Figure 6b). It is conceivable that the chains (Figure 7a) could be cut into blocks of different sizes than A and B and recombined in a way similar to what has been described before. In other words, an accretional series of chains can be imagined that, by combination, would result in a series of different 2D layers.

4. CONCLUSIONS

Both polymorphs of $Ba_2[UO_2(PO_4)_2]$ contain nonideal uranium environments: In α-$Ba_2[UO_2(PO_4)_2]$ (**1**) there is an edge-sharing PO_4 tetrahedron in addition to three corner-sharing PO_4 tetrahedra, leading to steric hindrance between one of the PO_4 oxygens [O(10)] and the uranyl oxygens O(9) and O(7). The resulting distances O(10)−O(9) and O(10)−O(7) correspond roughly to the minimum of the potential curve for pairs of nonbonded oxygens. The particular spatial distribution leads to bending of the uranyl group. The situation in β-$Ba_2[UO_2(PO_4)_2]$ (**2**) is simpler in that a similar interaction as in **1**, but with different spatial distribution, leads to tilting of the uranyl group with respect to the equatorial plane of the uranyl square bipyramids. The observed distortions of the uranyl polyhedra in both **1** and **2** are probably independent of any specific electronic property of the uranium atoms present.

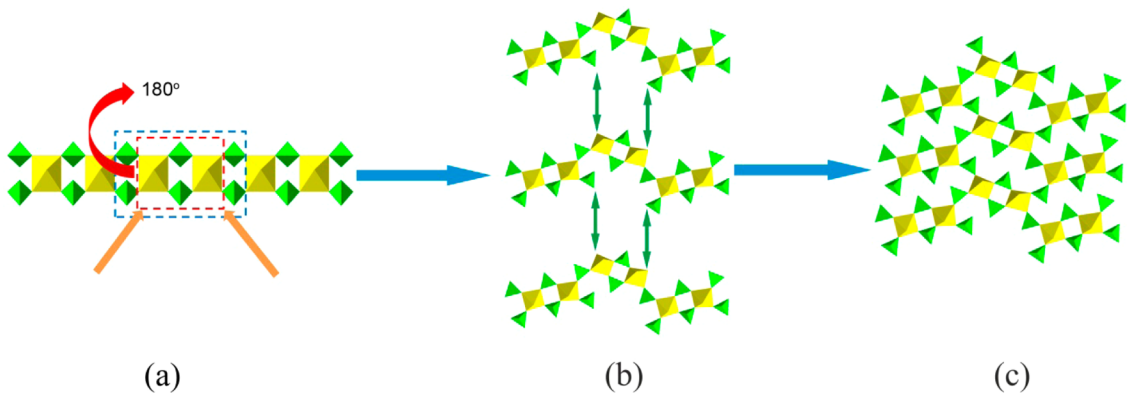

Figure 7. One/two-dimensional structural relationship between structural types of **2** and **3** (uranyl polyhedra are shown in yellow, TO_4 tetrahedra in green), and the proposed formation of one member of an accretional series.

dx.doi.org/10.1021/ic500965v | Inorg. Chem. 2014, 53, 7650−7660

It seems that there is a trade-off between **1** and **2** as both cations, UO_2^{2+} and Ba^{2+}, compete for bond valences from the phosphate oxygens. In **1**, the UO_2^{2+} gets an extra contribution by formation of a shared edge with one of the PO_4 tetrahedra at the expense of a smaller coordination number of the Ba atoms (9 or 10). In **2**, UO_2^{2+} does not have such an extra contribution, but the coordination number of Ba is higher, viz., 11.

These small differences, together with experimental evidence and the results of DFT calculations, suggest that both polymorphs represent two distinct minima on the free energy hyperplane, whereby the minimum of the α-phase is lower than that of the β-phase.

A structural relationship between the chain structure of **2** and the layer structure of **3** has been identified and the possibility of forming an accretional series is indicated.

■ ASSOCIATED CONTENT

Supporting Information

Three figures showing powder diffraction pattern of **1**, comparison of the coordination environment of uranium in **1** and $KNa_5(UO_2)(SO_4)_4{\cdot}H_2O$, and flexibility of the $UO_2(TO_4)_2$ (T = P, Mo, As) 1D chain in different inorganic compounds; eight tables listing atomic coordinates and displacement parameters for **1**−**3**, selected bond angles in **1**−**3**, distances between atoms to the least-square plane in **1**, **2**, and $KNa_5(UO_2)(SO_4)_4{\cdot}H_2O$, bond valence sums for cations in **1**−**3**; and crystallographic data and selected bond distances for **1** and **2**; X-ray crystallographic files in CIF format for **1**−**3**. This material is available free of charge via the Internet at http://pubs.acs.org.

■ AUTHOR INFORMATION

Corresponding Authors

*E-mail: albrecht-schmitt@chem.fsu.edu.
*E-mail: e.alekseev@fz-juelich.de.

Notes

The authors declare no competing financial interest.

■ ACKNOWLEDGMENTS

We are grateful for support provided by Deutsche Forschungsgemeinschaft for support within the DE 412/43-1 research project; by the Chemical Sciences, Geosciences, and Biosciences Division, Office of Basic Energy Sciences, Office of Science, Heavy Elements Program, U.S. Department of Energy, under Grant DE-SC0002215; by Helmholtz Association for the support within VH-NG-815 project; and by National Natural Sciences Foundation of China under Grant 41103055 and 41373106. Part of this research was funded by the Excellence Initiative of the German federal and state governments and the Jülich Aachen Research Alliance−High- Performance Computing. We thank the JARA-HPC awarding body for time on the RWTH computing cluster awarded through JARA-HPC Partition.

■ REFERENCES

(1) Burns, P. C. *Can. Mineral.* **2005**, *43*, 1839−1894.

(2) (a) Burns, P. C.; Deely, K. M.; Skanthakumar, S. *Radiochim. Acta* **2004**, *92* (3), 151−159. (b) Burns, P. C.; Klingensmith, A. L. *Elements* **2006**, *2* (6), 351−356.

(3) Burns, P. C. *Rev. Mineral. Geochem.* **1999**, *38*, 23−90.

(4) Hazen, R. M.; Ewing, R. C.; Sverjensky, D. A. *Am. Mineral.* **2009**, *94* (10), 1293−1311.

(5) (a) Wu, S.; Ling, J.; Wang, S.; Skanthakumar, S.; Soderholm, L.; Albrecht-Schmitt, T.; Alekseev, E.; Krivovichev, S.; Depmeier, W. *Eur. J. Inorg. Chem.* **2009**, 4039−4042. (b) Unruh, D. K.; Baranay, M.; Baranay, M.; Burns, P. C. *Inorg. Chem.* **2010**, *49* (15), 6793−6795. (c) Weng, Z.; Wang, S.; Ling, J.; Morrison, J. M.; Burns, P. C. *Inorg. Chem.* **2012**, *51* (13), 7185−7191.

(6) (a) Alekseev, E. V.; Krivovichev, S. V.; Depmeier, W. *Z. Anorg. Allg. Chem.* **2007**, *633*, 1125−1126. (b) Alekseev, E. V.; Krivovichev, S. V.; Malcherek, T.; Depmeier, W. *J. Solid State Chem.* **2008**, *181*, 3010−3015. (c) Alekseev, E. V.; Krivovichev, S. V.; Depmeier, W. *J. Solid State Chem.* **2009**, *182*, 2074−2080. (d) Alekseev, E. V.; Krivovichev, S. V.; Depmeier, W. *J. Mater. Chem.* **2009**, *19*, 2583−2587. (e) Alekseev, E. V.; Krivovichev, S. V.; Depmeier, W. *J. Solid State Chem.* **2009**, *182*, 2977−2984. (f) Alekseev, E. V.; Krivovichev, S. V.; Depmeier, W. *Cryst. Growth Des.* **2011**, *11*, 3295−3300. (g) Renard, C.; Obbade, S.; Abraham, F. *J. Solid State Chem.* **2009**, *182*, 1377−1386.

(7) Duisenberg, A. J. M.; Kroon-Batenburg, L. M. J.; Schreurs, A. M. M. *J. Appl. Crystallogr.* **2003**, *36*, 220−229.

(8) (a) Sheldrick, G. M. SADABS 2001, Program for absorption correction using SMART CCD, based on the method of Blessing.[8b] (b) Blessing, R. H. *Acta Crystallogr. A* **1995**, *51*, 33−38.

(9) Sheldrick, G. M. *Acta Crystallogr. A* **2008**, *64*, 112−122.

(10) (a) Frankowski, I.; Wachter, P. *Solid State Commun.* **1980**, *33* (8), 885−888. (b) Kotani, A.; Yamazaki, T. *Prog. Theor. Phys. Suppl.* **1992**, *108*, 117−131.

(11) (a) Dorado, B.; Amadon, B.; Freyss, M.; Bertolus, M. *Phys. Rev. B* **2009**, *79*, No. 235125. (b) Rák, Zs.; Ewing, R. C.; Becker, U. *Phys. Rev. B* **2011**, *84*, No. 155128.

(12) Giannozzi, P.; Baroni, S.; Bonini, N.; et al. *J. Phys.: Condens. Matter* **2009**, *21*, No. 395502.

(13) (a) Perdew, J. P.; Burke, K.; Ernzerhof, M. *Phys. Rev. Lett.* **1996**, *77*, 3865−3868. (b) Perdew, J. P.; Burke, K.; Ernzerhof, M. *Phys. Rev. Lett.* **1997**, *78*, 1396E. (c) Perdew, J. P.; Ruzsinszky, A.; Csonka, G. I.; Vydrov, O. A.; Scuseria, G. E.; Constantin, L. A.; Zhou, X.; Burke, K. *Phys. Rev. Lett.* **2008**, *100*, No. 136406.

(14) Schreckenbach, G.; Shamov, G. A. *Acc. Chem. Res.* **2010**, *43*, 19−29.

(15) Methfessel, M.; Paxton, A. T. *Phys. Rev. B* **1989**, *40*, 3616−3621.

(16) Vanderbilt, D. *Phys. Rev. B* **1990**, *41*, 7892−7895.

(17) (a) Jing, F.; Wu, Y.; Fu, P. *J. Cryst. Growth* **2006**, *292* (2), 454−457. (b) Yan, W.; Wang, L.; Xia, Z.; Cheng, M.; Li, Q.; Zhang, Y. *Mater. Res. Bull.* **2007**, *42* (8), 1468−1472. (c) Yue, Y.; Hu, Z.; Chen, C. *J. Cryst. Growth* **2008**, *310* (6), 1264−1267. (d) Zhu, C.; Li, W.; Nai, X.; Zhu, D.; Guo, F.; Song, S. *Cryst. Res. Technol.* **2012**, *47* (1), 73−78.

(18) (a) Gasperin, M. *Acta Crystallogr. C* **1987**, *43*, 2031−2033. (b) Gasperin, M. *Acta Crystallogr. C* **1987**, *43*, 1247−1250. (c) Gasperin, M. *Acta Crystallogr. C* **1987**, *43*, 2264−2266. (d) Gasperin, M. *Acta Crystallogr. C* **1988**, *44*, 415−416. (e) Gasperin, M. *Acta Crystallogr. C* **1989**, *45*, 981−983. (f) Gasperin, M. *Acta Crystallogr. C* **1990**, *46*, 372−374. (g) Cousson, A.; Gasperin, M. *Acta Crystallogr. C* **1991**, *47*, 10−12. (h) Gasperin, P. M.; Rebizant, J.; Dancausse, J. P.; Meyer, D.; Cousson, A. *Acta Crystallogr. C* **1991**, *47*, 2278−2279.

(19) (a) Wang, S.; Alekseev, E. V.; Depmeier, W.; Albrecht-Schmitt, T. E. *Chem. Commun.* **2010**, *46* (22), 3955−3957. (b) Wang, S.; Alekseev, E. V.; Diwu, J.; Casey, W. H.; Phillips, B. L.; Depmeier, W.; Albrecht-Schmitt, T. E. *Angew. Chem., Int. Ed.* **2010**, *49* (6), 1057−1060. (c) Wang, S.; Alekseev, E. V.; Ling, J.; Liu, G.; Depmeier, W.; Albrecht-Schmitt, T. E. *Chem. Mater.* **2010**, *22* (6), 2155−2163. (d) Wang, S.; Alekseev, E. V.; Ling, J.; Skanthakumar, S.; Soderholm, L.; Depmeier, W.; Albrecht-Schmitt, T. E. *Angew. Chem., Int. Ed.* **2010**, *49* (7), 1263−1266. (e) Wang, S.; Alekseev, E. V.; Miller, H. M.; Depmeier, W.; Albrecht-Schmitt, T. E. *Inorg. Chem.* **2010**, *49* (21), 9755−9757. (f) Wang, S.; Alekseev, E. V.; Stritzinger, J. T.; Depmeier, W.; Albrecht-Schmitt, T. E. *Inorg. Chem.* **2010**, *49* (14), 6690−6696. (g) Wang, S.; Alekseev, E. V.; Stritzinger, J. T.; Depmeier, W.; Albrecht-Schmitt, T. E. *Inorg. Chem.* **2010**, *49* (6), 2948−2953. (h) Wang, S.; Alekseev, E. V.; Stritzinger, J. T.; Liu, G.; Depmeier, W.; Albrecht-Schmitt, T. E. *Chem. Mater.* **2010**, *22* (21), 5983−5991. (i) Wang, S.; Alekseev, E. V.; Depmeier, W.; Albrecht-Schmitt, T. E. *Chem. Commun.* **2011**, *47* (39),

10874−10885. (j) Wang, S.; Alekseev, E. V.; Diwu, J.; Miller, H. M.; Oliver, A. G.; Liu, G.; Depmeier, W.; Albrecht-Schmitt, T. E. *Chem. Mater.* **2011**, *23* (11), 2931−2939. (k) Wang, S.; Villa, E. M.; Diwu, J.; Alekseev, E. V.; Depmeier, W.; Albrecht-Schmitt, T. E. *Inorg. Chem.* **2011**, *50* (6), 2527−2533. (l) Wang, S.; Alekseev, E. V.; Depmeier, W.; Albrecht-Schmitt, T. E. *Inorg. Chem.* **2011**, *50* (11), 4692−4694. (m) Wang, S.; Alekseev, E. V.; Depmeier, W.; Albrecht-Schmitt, T. E. *Inorg. Chem.* **2011**, *50* (6), 2079−2081. (n) Polinski, M. J.; Wang, S.; Alekseev, E. V.; Depmeier, W.; Albrecht-Schmitt, T. E. *Angew. Chem., Int. Ed.* **2011**, *50* (38), 8891−8894. (o) Polinski, M. J.; Wang, S.; Cross, J. N.; Alekseev, E. V.; Depmeier, W.; Albrecht-Schmitt, T. E. *Inorg. Chem.* **2012**, *51* (14), 7859−7866.

(20) Wu, S.; Wang, S.; Diwu, J.; Depmeier, W.; Malcherek, T.; Alekseev, E. V.; Albrecht-Schmitt, T. E. *Chem. Commun.* **2012**, *48* (29), 3479−3481.

(21) (a) Burns, P. C.; Hayden, L. A. *Acta Crystallogr. C* **2002**, *58*, i121−i123. (b) Hayden, L. A.; Burns, P. C. *J. Solid State Chem.* **2002**, *163*, 313−318. (c) Hayden, L. A.; Burns, P. C. *Can. Mineral.* **2002**, *40*, 211−216.

(22) Hyde, B. G.; Sellar, J. R.; Stenberg, L. *Acta Crystallogr.* **1986**, *B42*, 423−429.

(23) Burns, P. C.; Ewing, R. C.; Hawthorne, F. C. *Can. Mineral.* **1997**, *35*, 1551−1570.

(24) Brese, N. E.; O' Keeffe, M. *Acta Crystallogr. B* **1991**, *47*, 192−197.

(25) Fischer, K.; Puchelt, H. Barium. In *Handbook of Geochemistry*; Springer-Verlag: Berlin and Heidelberg, Germany, 1972; Chapt. 56.

(26) Haas, P.; Tran, F.; Blaha, P.; Schwarz, K. *Phys. Rev. B* **2011**, *83*, 205117.

(27) Adllan, A. A.; Dal Corso, A. *J. Phys.: Condens. Matter.* **2011**, *23* (42), 425501.

(28) Iche-Tarat, N.; Marsden, C. J. *J. Phys. Chem. A* **2008**, *112*, 7632−7643.

(29) Krivovichev, S. V.; Burns, P. C.; Tananaev, I. G., Eds. *Structural Chemistry of Inorganic Actinide Compounds*; Elsevier: Amsterdam, 2007.